

Control of cerebral ischemia with magnetic nanoparticles

Jie-Min Jia¹, Praveen D Chowdary², Xiaofei Gao¹, Bo Ci¹, Wenjun Li³, Aditi Mulgaonkar⁴, Erik J Plautz⁵, Gedaa Hassan⁴, Amit Kumar⁴, Ann M Stowe⁵, Shao-Hua Yang³, Wei Zhou⁶, Xiankai Sun⁴, Bianxiao Cui² & Woo-Ping Ge^{1,7-9}

The precise manipulation of microcirculation in mice can facilitate mechanistic studies of brain injury and repair after ischemia, but this manipulation remains a technical challenge, particularly in conscious mice. We developed a technology that uses micromagnets to induce aggregation of magnetic nanoparticles to reversibly occlude blood flow in microvessels. This allowed induction of ischemia in a specific cortical region of conscious mice of any postnatal age, including perinatal and neonatal stages, with precise spatiotemporal control but without surgical intervention of the skull or artery. When combined with longitudinal live-imaging approaches, this technology facilitated the discovery of a feature of the ischemic cascade: selective loss of smooth muscle cells in juveniles but not adults shortly after onset of ischemia and during blood reperfusion.

Stroke is the second leading cause of death worldwide, killing nearly 6.7 million individuals each year. Of these individuals, 80% have accompanying ischemia that deprives brain cells of oxygen and nutrients¹. To understand the molecular and cellular mechanisms of brain injury and repair after ischemic stroke, multiple approaches have been used to produce focal ischemia via occlusion mediated with a suture or ligation²⁻⁵, thrombotic blood clot emboli^{6,7}, dye-induced photothrombosis (e.g., using Rose-Bengal or erythrosine B)⁸⁻¹⁰, and occlusion mediated through endothelin-1 (refs. 2,11,12). Furthermore, thrombosis can be introduced by inducing focal occlusion in single microvessels with a green or infrared laser¹³⁻¹⁵. However, the various procedures either require overly invasive surgery or do not allow precise control of reperfusion in blood vessels, especially in microvessels^{2,12,16}. Hence, it remains challenging to induce focal ischemia that encompasses accurate manipulation of stroke size and duration of ischemia to probe the disruption of the neuron–glia–vasculature network. Here, we report the development of an approach to induce focal ischemia with precise control of infarct size and occlusion duration. The occlusion, which is reversible, is achieved via micro-

magnet-mediated aggregation of magnetic particles (MPs) within microvessels (Fig. 1a–c). In combination with longitudinal live imaging, our approach allows the investigation of the disruption and repair of neurovascular units *in vivo* under ischemic stroke.

RESULTS

Properties of magnetic particles

To utilize magnetic force to achieve microvessel occlusion, we produced various superparamagnetic nanoparticles. We then used empirically determined magnetic gradients to effect localized nanoparticle aggregation (Supplementary Fig. 1). Both the size and coating material of MPs can affect their biocompatibility, solubility, toxicity, and circulation time; nanoparticles of <10 nm or >200 nm are quickly cleared from circulation via the reticuloendothelial system¹⁷. MPs coated with polyethylene glycol (PEG) or dextran exhibit good biocompatibility, a long circulation time, and low toxicity¹⁸. To further reduce toxicity in mice, we tested MPs of 10–200 nm diameter coated with various materials including PEG-200, PEG-2000, dextran, and silica. Our *in vivo* tests demonstrated that 180-nm MPs (176.57 ± 1.52 nm, *n* = 6 measurements) coated with PEG-2000 were best suited for mediating blood occlusion in live animals. The MPs were superparamagnetic with high-saturation magnetization (54 emu/g) and low remanence (2.7 emu/g), which proved important for the reversibility of occlusion when the micromagnets were removed from the occlusion site (Supplementary Fig. 1). In HEK293T cells and astrocytes, 1 or 2 mg/ml PEG-2000-coated 180-nm MPs had no effect on cell viability (Supplementary Figs. 2 and 3). Tail-vein injection of the 180-nm MPs (dose, 100 µg MPs per g body weight) into the bloodstream of mice (*n* = 54, postnatal days (P) 17–365) did not lead to mortality, although we observed that most of the MPs went to the liver and spleen within 2 h postinjection (Supplementary Fig. 4). Further, no significant difference between control and injected animals was detected in mouse respiratory rate, body temperature, heart rate, blood oxygen saturation (SpO₂), body weight, blood carbon dioxide

¹Children's Research Institute, University of Texas Southwestern Medical Center, Dallas, Texas, USA. ²Department of Chemistry, Stanford University, Stanford, California, USA. ³Center for Neuroscience Discovery, University of North Texas Health Science Center, Fort Worth, Texas, USA. ⁴Department of Radiology, University of Texas Southwestern Medical Center, Dallas, Texas, USA. ⁵Department of Neurology and Neurotherapeutics, University of Texas Southwestern Medical Center, Dallas, Texas, USA. ⁶Britton Chance Center for Biomedical Photonics, Wuhan National Laboratory for Optoelectronics-HuaZhong University of Science and Technology, Wuhan, China. ⁷Department of Pediatrics, University of Texas Southwestern Medical Center, Dallas, Texas, USA. ⁸Department of Neuroscience, University of Texas Southwestern Medical Center, Dallas, Texas, USA. ⁹Harold C. Simmons Comprehensive Cancer Center, University of Texas Southwestern Medical Center, Dallas, Texas, USA. Correspondence should be addressed to W.-P.G. (woo-ping.ge@utsouthwestern.edu) or B. Cui (bcui@stanford.edu).

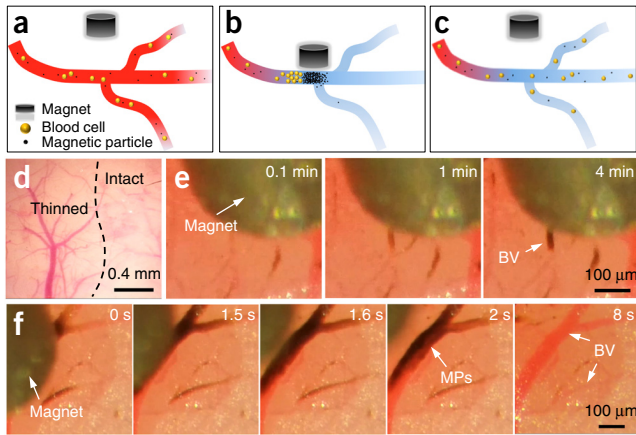


Figure 1 | Reversible occlusion in microvessels produced with magnetic nanoparticles. (a–c) Strategy used to occlude blood vessels through aggregation of MPs. Once a magnet approaches a blood vessel, MPs accumulate to form an occlusion. Occlusion is reversed when the magnet is moved away from a blood vessel. Red indicates normal oxygen and nutrients. Blue indicates low oxygen and nutrients in blood. (d–f) Timecourse of MP aggregation in microvessels in the cerebral cortex. (d) An image of blood vessels under thinned skull. (e) Microvessel occlusion was achieved with a 0.5-mm micromagnet. An occlusion was formed approximately 4 min after the magnet was close to the skull. (f) Reperfusion after magnet removal.

(ECO_2), and blood glucose (Supplementary Figs. 5 and 6). These *in vitro* and *in vivo* tests demonstrated that PEG-2000-coated 180-nm MPs did not notably affect mouse health or basic physiological properties.

To test whether MPs cause an inflammatory response in the brain, we injected $10\ \mu\text{g}$ MPs into the hippocampal region of one hemisphere in *CX3CR1-GFP* knock-in mice, in which microglia in the brain express GFP¹⁹. As a control, we injected the contralateral hemisphere with the same volume of phosphate-buffered saline (PBS; $1\ \mu\text{l}$). The morphology and cell density of microglia did not differ between the experimental and control hemispheres at 5–7 d after MP injection (Supplementary Fig. 7). Similar experiments were performed in *Thy1-tdTomato* transgenic mice, in which pyramidal neurons are specifically labeled with tdTomato. There was no significant difference in neuronal morphology and spine density in dendrites (Supplementary Fig. 8). These experiments demonstrated that PEG-2000-coated 180-nm MPs do not elicit an inflammatory response in the brain.

Properties of micromagnets

To achieve localized field gradients and produce occlusion with high spatiotemporal specificity, we produced cylindrical magnets made of neodymium–iron–boron (NdFeB), which is one of the strongest permanent magnetic materials²⁰; the magnets were 1–2 mm long and of differing diameter (0.3–3.0 mm, Supplementary Fig. 1). The magnetic field induction was measured along the cylindrical axis. The magnetic field profiles of all magnets were in good agreement with scaled theoretical profiles obtained using an analytical formula (Supplementary Fig. 1). We then computed the magnetic field gradients and relative forces of different magnet geometries that could be exerted on the 180-nm MPs at different distances from the face of the magnet (Supplementary Fig. 1). Whereas steeper gradients and greater forces were achievable in

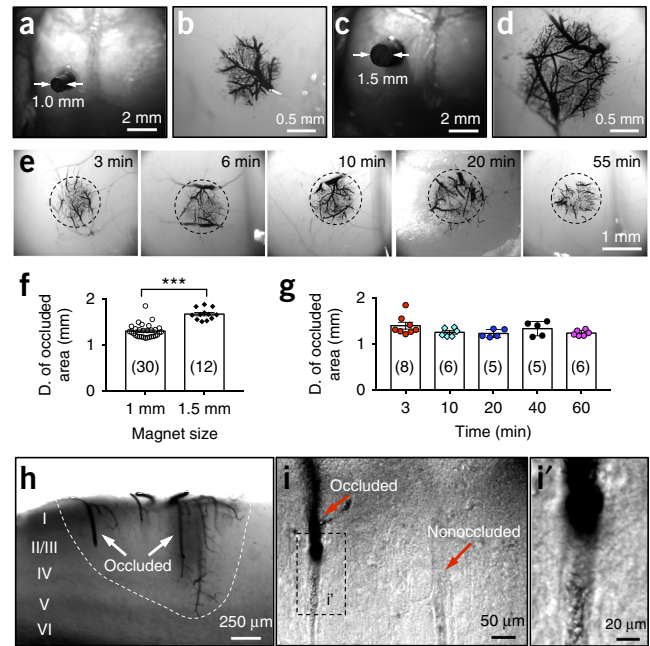


Figure 2 | Precise control of occlusion size with magnetic nanoparticles. (a–d) Targeting of an occlusion to a focal brain region. A magnet (diameter 1.0 or 1.5 mm) was glued on a mouse skull before injection of MPs into the tail vein. The dark regions in (b) and (d) indicate aggregation of MPs in blood vessels. (e) MP aggregation in blood vessels at different timepoints. We placed a magnet for the indicated times on the mouse skull without skull thinning. Images of brains were taken after mice were euthanized, followed by the removal of their skulls. Each dashed circle denotes the occluded region. (f) Summary of results for the diameter of the occluded region produced with two different magnets, 1.0 and 1.5 mm. D., diameter. (g) Summary of results for the diameter of the occluded region with a 1-mm magnet with different duration of occlusion. The 3-min and 60-min groups represent the 3- to 7-min and 50- to 60-min occlusion, respectively. The number indicated for each point is the number of mice used for each group. (h) Images from a coronal section of the brain shown in e. I–VI represent the six cortical layers. The dark areas indicate the occluded blood vessels. Brain region occupied by occluded blood vessels is denoted with a dashed line. (i) High-magnification image of two penetrating blood vessels in the cerebral cortex. One was occluded (left), whereas the other was not occluded (right). (i') Inset from i. High-magnification image of the occluded blood vessel in i. ***, $P < 0.001$; two-tailed unpaired *t*-test. All error bars indicate s.e.m.

close proximity to the smaller magnets, the larger magnets had greater effective reach owing to a slower decay of the gradient and force with increasing distance from the magnet face (Supplementary Fig. 1). Therefore, we used magnets of different sizes depending on the diameter of the artery to be occluded (Supplementary Table 1).

Reversible occlusion in microvessels produced with magnetic nanoparticles

For the 0.3- and 0.5-mm magnets, we found that $\sim 300\ \mu\text{m}$ was the effective working distance (nominally defined as the distance at which the force was $\sim 20\%$ of its value at the magnet face). This short range of magnetic force provided high spatial specificity for effecting focal occlusion (Supplementary Fig. 1). To test whether our micromagnets could be used to reversibly occlude microvessels, we approached microvessels with the 0.3- or 0.5-mm micromagnet through a manipulator so that imaging and occlusion could be performed simultaneously after tail-vein injection of 1–2 mg

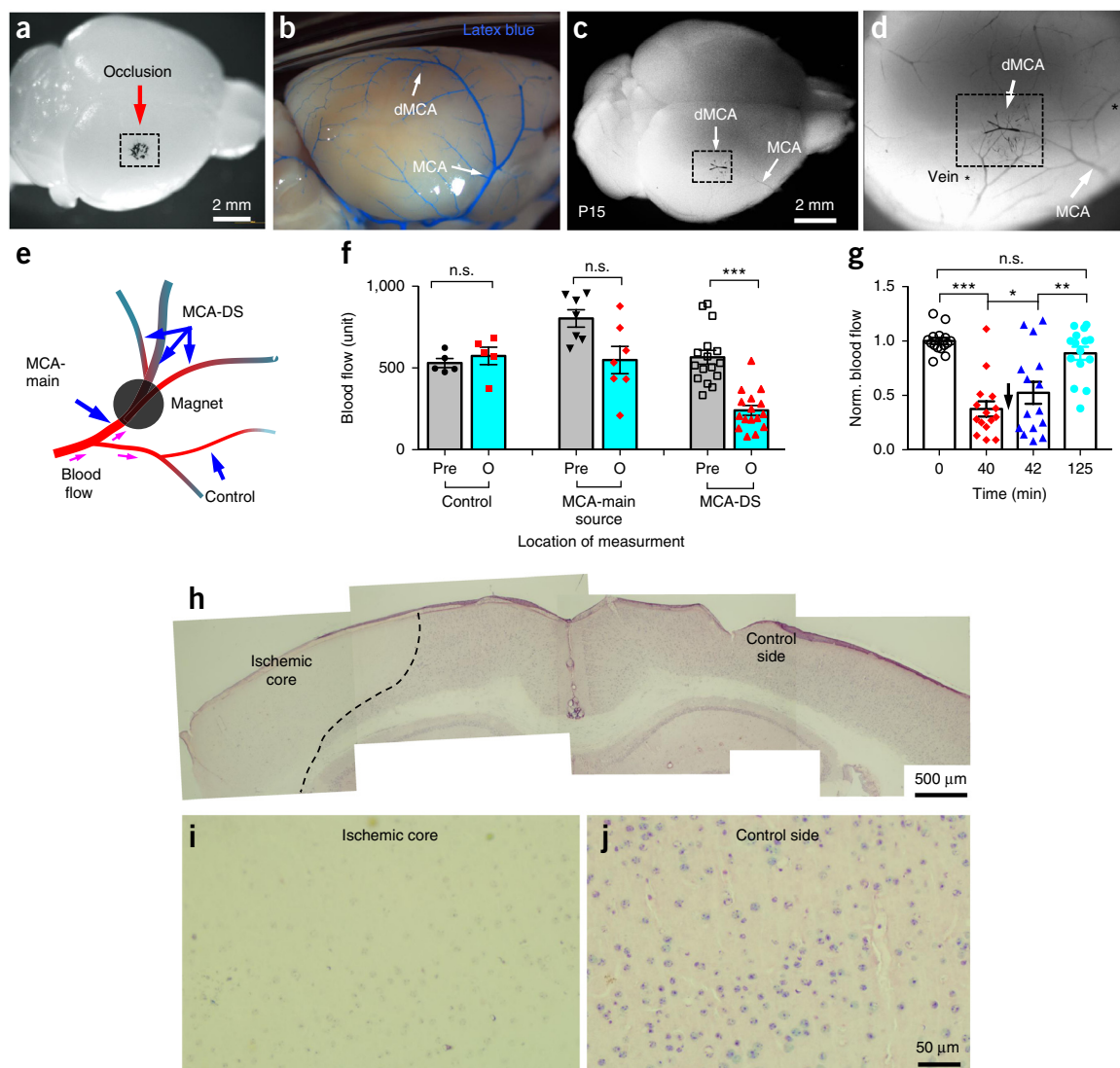


Figure 3 | MP-mediated occlusion in cortical blood vessels of perinatal and neonatal mice and distal middle carotid artery (MCA). **(a)** Occlusion in blood vessels of the perinatal mouse brain with a 1-mm magnet. The mouse (P3) skull remained intact. MPs were administered via injection from the superficial temporal vein. **(b)** MCA and its distal branches (dMCA) are shown after brain vasculature was perfused with latex blue. **(c)** MP-mediated occlusion after a magnet was placed above dMCA on the skull of a P15 mouse. **(d)** The brain with MP-mediated occlusion in **(c)** was imaged under a dissection microscope. Black, MPs in dMCA. **(e)** Model demonstrating where a magnet was placed for MP-mediated occlusion of MCA. Magenta arrows, blood flow direction. **(f)** Blood flow (juvenile and adult, see **Supplementary Table 1**) was measured by laser Doppler flowmetry at the locations shown in **(e)**. Control, blood flow in locations ~2–5 mm away from the magnet. MCA-main (source), upstream MCA adjacent to the magnet. MCA-DS, downstream MCA adjacent to the magnet. **(g)** Blood flow (P15–25, juvenile mice) in MCA-main and MCA-DS was measured by laser Doppler flowmetry before occlusion (0 min), after a 40-min occlusion (40 min), 2 min after magnet removal (42 min), and 100–150 min after the baseline was measured (125 min). We removed the magnet from mouse skull at 40 min (arrow). Baseline, $100.0 \pm 3.0\%$; 40 min after occlusion, $37.6 \pm 7.2\%$; 2 min after magnet removal, i.e. 42 min, $52.5 \pm 14.0\%$; 125 min, $88.8 \pm 6.3\%$. **(h–j)** Hematoxylin and eosin staining of brain sections with MP-mediated occlusion for 2 h in dMCA (as shown in **(g)**) followed by 6-d reperfusion in an adult mouse. **(h)** is a composite image. * $P < 0.05$; ** $P < 0.01$; *** $P < 0.001$; n.s., not significant; two-tailed unpaired t -test. All error bars indicate s.e.m.

of 180-nm MPs. Owing to the short working distance of the micro-magnet for aggregating the MPs, the occlusion experiments were initially performed under thinned-skull preparation (**Fig. 1d**). Blood flow in microvessels was occluded within minutes (**Fig. 1e**). This was consistent with our *in vitro* tests, which showed MP aggregation within 4 min after a 0.3-mm micromagnet was placed ~545 μm away from suspended MPs within a 100- μm film of solution (**Supplementary Fig. 1**). Importantly, we could achieve blood reperfusion upon removal of the magnet (**Fig. 1f** and **Supplementary Video 1**). These experiments demonstrated that

magnetic force could be used to achieve precise spatiotemporal manipulation of blood flow in microvessels.

Focal blood occlusion produced in awake mice with the intact skull

In past rodent experiments, invasive surgery (arteries or skull) was required if researchers wanted to produce focal ischemia in the brain^{2,12,16}. To test whether we could produce focal blood occlusion in mice without skull thinning, we measured occlusion size (i.e., the diameter of the region with blood vessels occluded by

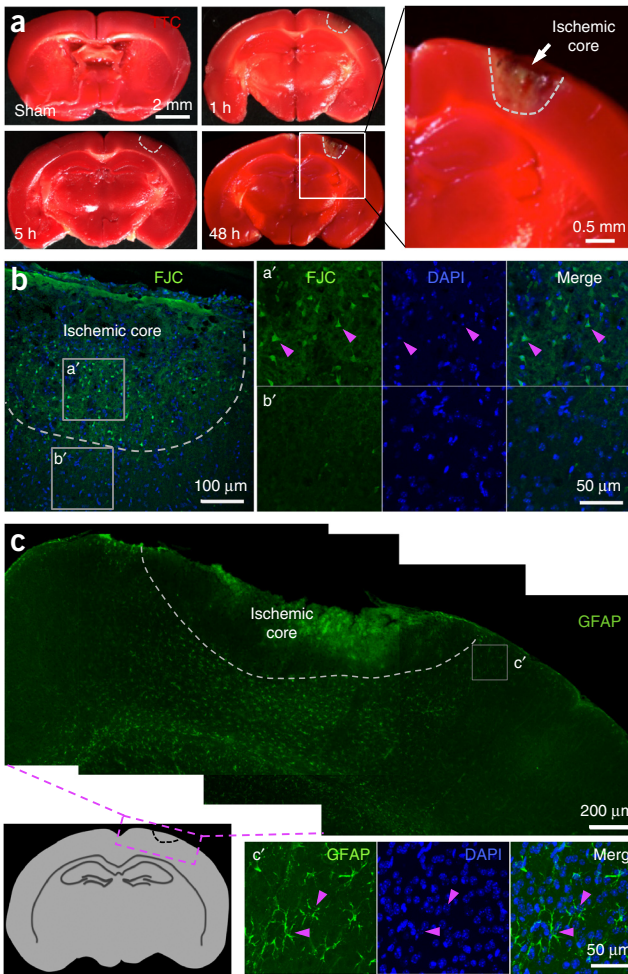


Figure 4 | Ischemic stroke can be induced through aggregation of MPs. (a) TTC staining of brain slices from mice (>P50) after 0, 1, 5, or 48 h of MP-mediated occlusion. The occlusion was produced with a 1.5-mm magnet. Inset, ischemic region 48 h after MP-mediated occlusion. Each ischemic region is denoted with a dashed line. (b) Brain sections were labeled with Fluoro Jade C (FJC) at 48 h after MP-mediated occlusion. (a',b') Insets from (b), a region from ischemic core (a') and peri-infarct region (b'). Green dots denote degenerated neurons (arrowheads) stained by FJC. The degenerated neurons have shrunken nuclei (DAPI, blue, arrowheads). (c) Activated astrocytes marked by expression of GFAP, magenta arrowheads) around the ischemic region. (c'), insets from c. Panel c is a composite image. Blue, nuclei stained with DAPI.

MPs) after applying a magnet (diameter, 1 or 1.5 mm) to the intact mouse skull (juvenile mice, P15–P25) with only the skin removed (Fig. 2a–d). We achieved blood vessel occlusion in the cerebral cortex even in conscious or motile mice. Occlusion size depended on magnet diameter (Fig. 2b,d–f). Blood vessel occlusion was achieved within 3–5 min (Fig. 2e). The size of the occluded area was stable over 5 h if the magnets were not removed (Fig. 2g). To induce stable blood occlusion in adult mice, we usually performed our experiments with thinned-skull preparation (~50 μm in thickness) because their skulls are thicker (117.5 ± 5.5 μm for P60–P75, $n = 4$ mice; 186.2 ± 4.3 μm for P360–P370, $n = 6$) than those of juvenile mice (68.8 ± 4.4 μm for P16–P27, $n = 12$). Postocclusion sectioning of fixed brains revealed that blood vessels could be occluded in both superficial and deep layers of the cerebral cortex

(Fig. 2h,i). In contrast to other approaches that usually require anesthesia to produce focal ischemia in mice, our methodology allows the facile generation of occlusion in a focal brain region of awake or motile mice without anesthesia or open-skull surgery.

Focal blood occlusion produced in perinatal and neonatal mice and distal middle carotid artery

Because of their small size and low body weight (1–6 g), the diameter of arteries in perinatal (P0–P3) and neonatal (P4–P9) mice is small compared with those in juvenile and adult mice. It is technically challenging to do surgeries in arteries of perinatal mice (body weight 1–2 g) with conventional methods—for example, middle cerebral artery occlusion (MCAO)—to generate reversible focal ischemia. Even for P7–P9 neonatal mice, surgical manipulation of arteries is difficult^{21,22}. Researchers usually use neonatal rats as models to mimic neonatal stroke because of the rats' large body weights²³. Our results demonstrated that we could use MPs to induce blood occlusion in a focal brain region in perinatal and neonatal mice with their skulls intact (Fig. 3a). With magnetic force, we could form an occlusion in distal branches of MCA (Fig. 3b–d). To evaluate the extent of occlusion, we used laser Doppler flowmetry to measure the blood flow before and after the MPs accumulated. We found that blood flow speed in downstream branches of main middle carotid arteries (MCAs) decreased substantially after MP-mediated occlusion in juvenile mice as well as in adult mice ($43.2 \pm 5.2\%$ of baseline; Fig. 3e,f). Hematoxylin and eosin staining further validated that the occlusion led to ischemic injury in the cortical region (Fig. 3h–j). Reperfusion was achieved when the magnets were removed from the mouse skull ($n = 15$ MCA branches, P15–P25; Fig. 3e,g). In short, our approach for focal ischemia could be applied to mice of any postnatal age; in particular, it could generate distal MCAO in perinatal and neonatal mice.

Ischemic stroke can be induced through aggregation of magnetic particles

To assess whether MP-mediated blood occlusion could lead to ischemia-induced neuronal degeneration, we stained fresh brain slices with 2,3,5-triphenyltetrazolium chloride (TTC) as reported²⁴. We observed occluded regions—as indicated by weak red staining owing to impaired mitochondrial activity—at 1, 5, and 48 h after occlusion (Fig. 4a, magnets remained on skull). We also detected degenerated neurons (stained by Fluoro Jade C²⁵) and disrupted blood vessels in ischemic regions (Fig. 4b and Supplementary Fig. 9). Further, a large number of activated astrocytes exhibited upregulated glial fibrillary acidic protein (GFAP) expression in peri-infarct zones (Fig. 4c), which has been reported in ischemic regions²⁶. These results indicated that MP-mediated occlusion can induce ischemic injury. We named this approach 'stroke induced with magnetic particles' (SIMPLE) owing to its convenience and reliable production of focal ischemic stroke in mouse brain (Figs. 1–4).

Smooth muscle cells during occlusion and after reperfusion

Neurons, astrocytes, and vascular cells coordinate with each other to form the neurovascular unit and maintain brain metabolic activity^{27,28}. Located in arteries and arterioles, smooth muscle cells (SMCs) provide structural integrity to the neurovascular unit and regulate vascular diameter by contracting and relaxing

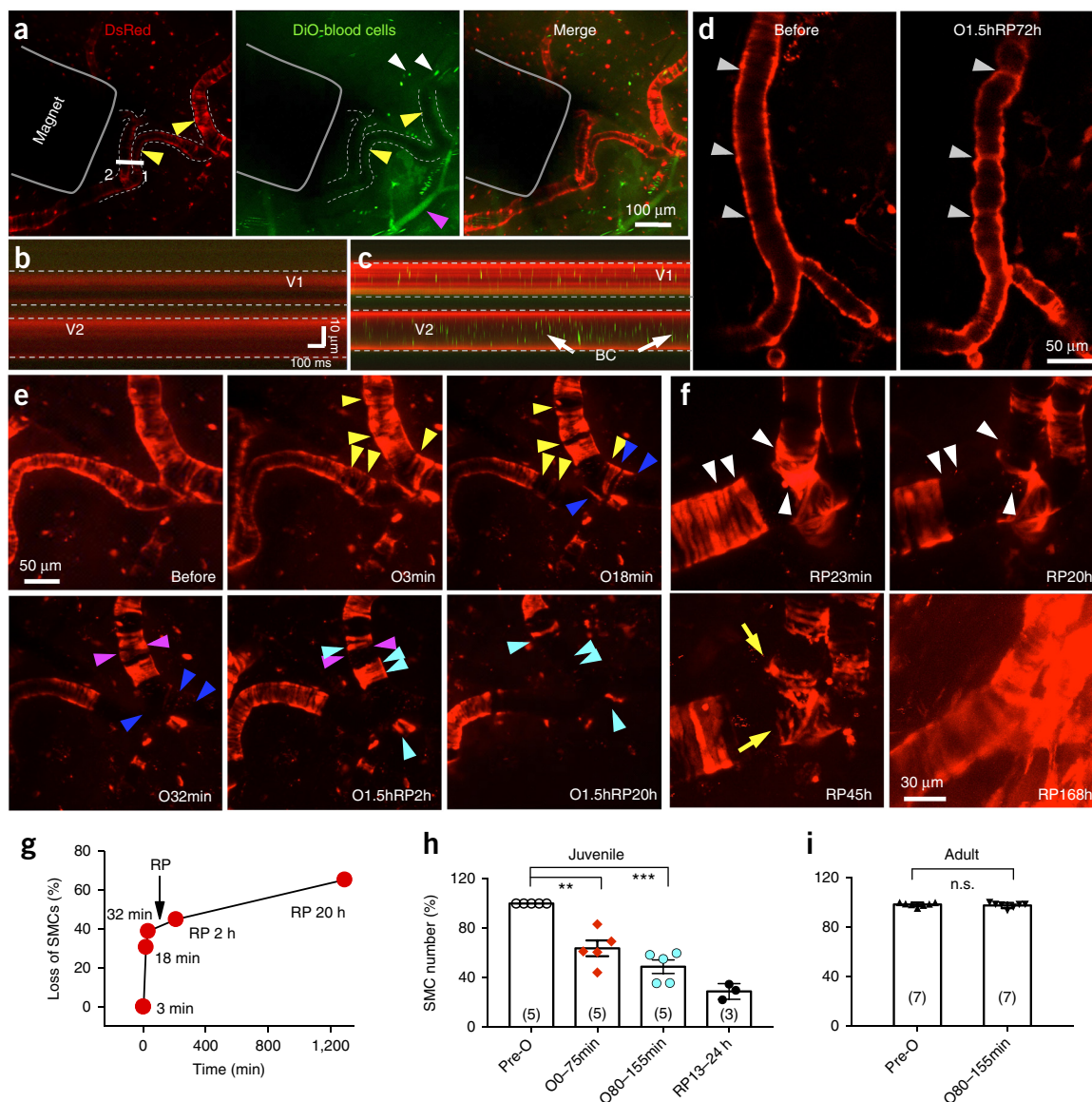


Figure 5 | Loss of SMCs during occlusion and after reperfusion. **(a)** Occlusions in two small arteries (yellow arrowheads) were produced with a micromagnet (diameter 0.3 mm) under a two-photon excitation microscope. Blood cells were labeled with DiO (green). SMCs were labeled with DsRed in *NG2DsRedBACtg* mice. Magenta arrowhead, nonoccluded vessels. White arrowheads, flowing individual blood cells. Areas within the dashed lines indicate arteries that were occluded with MPs. Numbers 1 and 2 indicate arteries. **(b,c)** Line scanning of two small arteries in the location marked with a white bar in **a**. Occlusion **(b)** and reperfusion **(c)** in two arteries (dashed lines). Green, blood cells labeled with DiO. Red, DsRed fluorescence in *NG2DsRedBACtg* mice. V1 and V2 indicate arteries 1 and 2 in **a**. **(d)** A small artery from an adult mouse brain before and during a constriction. Arrowheads, constricted locations. O1.5hRP72h, 1.5-h occlusion with subsequent 72-h reperfusion. **(e)** Images of SMCs at different timepoints from two small arteries under ischemia and after reperfusion. Before, before occlusion; O3min, O18min, and O32min indicate 3, 18, and 32 min (respectively) after occlusion; O1.5hRP2h, 1.5-h occlusion with subsequent 2-h reperfusion; O1.5hRP20h, 1.5-h occlusion with subsequent 20-h reperfusion. Lost SMCs are indicated by variously colored arrowheads in these images. The same set of arrowheads in the two images denotes SMCs that were lost at two different timepoints. **(f)** SMCs in an injured artery or arteriole after a 1.5-h occlusion with MPs. Images were taken at different timepoints after reperfusion (RP). Arrowheads, sites of SMC loss; arrows, repaired SMCs. **(g)** Percentage of lost SMCs during occlusion and after reperfusion in arteries from the juvenile mouse in **f**. **(h)** Summary of results ($n = 5$ mice for each timepoint) for arteries under different conditions from juvenile mice. Pre-O, before MP-mediated occlusion; O0-75min, occlusion within 75 min; O80-155min, during 80-155 min of occlusion; RP13-24 h, during reperfusion for 13-24 h. All data were normalized to the number of SMCs before occlusion. **(i)** Summary of results for arteries under different conditions from adult mice ($n = 5$). n.s., not significant, $P > 0.05$; *, $P < 0.05$; **, $P < 0.01$; ***, $P < 0.001$; two-tailed unpaired t -test (compared with Pre-O group). All error bars indicate s.e.m.

in response to vasoactive stimuli²⁹. Most of the attention concerning ischemic stroke has focused on neurons, and little is known about the involvement of SMCs under ischemic injury—especially in the developing brain³⁰. SIMPLE provided a suitable strategy to reversibly manipulate blood occlusion in mice at different devel-

opmental ages to assess SMC dynamics during occlusion and after reperfusion. To measure blood flow in microvessels, we used DiO dye to label cells from a small amount of whole blood (~10–20 μ l; see details in Online Methods) and then injected them back into the same mouse via tail vein. To target microvessels, we held a

magnet with a glass capillary and moved it near a small artery or arteriole with a manipulator (Fig. 5a). With time-lapse imaging (Supplementary Video 2) and line scanning, we quantified and analyzed blood flow speed in a single arteriole or artery (Fig. 5b,c). We visualized SMCs in the transgenic mouse strain *NG2DsRedBAC*, in which SMCs are genetically labeled with the fluorescent protein DsRed^{31,32}. SMCs were distinguishable because of their characteristic ring-like structure and were labeled by an antibody against an SMC-specific antigen (α -smooth-muscle actin, α SMA; Supplementary Figs. 10 and 11). After performing occlusion of arteries, we frequently observed constricting SMCs under ischemia (Fig. 5d, P100–P365, $n = 5$), which is consistent with a recent report concerning adult mice³². SIMPLE therefore provides a potential strategy to produce focal ischemia with reliable duration of occlusion in juvenile mice (P15–P25, 8–12 g body weight) for live-imaging studies, which remains a challenge with conventional approaches in mice. For juvenile mice, we observed that a high percentage of SMCs were lost (i.e., loss of DsRed fluorescence) shortly after arteries were fully occluded (Fig. 5e); this loss likely indicated SMC death because we did not observe SMC re-emergence in these regions even 20 or 45 h after reperfusion (Fig. 5f). As an example, in a P20 brain we observed substantial SMC loss (30.6%) within 18 min after occlusion, and an additional 20.4% SMC loss occurred during the 20-h reperfusion period (Fig. 5e–g). Although the severity of loss varied among mice, 17–55% (mean, $36.2 \pm 7.1\%$; $n = 5$ mice) of SMCs were lost in arteries or arterioles within 75 min postocclusion (Fig. 5h). Within the 155-min occlusion period, more than half of SMCs were lost (mean, $51.1 \pm 6.2\%$, $n = 5$ mice; Fig. 5h and Supplementary Video 3). Taking advantage of the reversibility of SIMPLE, we removed the magnet, and the occluded vessels reperfused. We observed SMC loss up to 71.1% during reperfusion (<1 d, $n = 3$ mice; Fig. 5h). Compared with the occlusion stage, more severe damage is believed to occur during reperfusion after ischemic stroke²⁹. However, our results demonstrate that more SMCs were lost during occlusion than during reperfusion. The severe SMC loss induced by occlusion was observed in juvenile mice but not adult mice (Fig. 5i). After the removal of micromagnets after a 1.5-h occlusion, we observed the recovery of SMCs in the injured blood vessels 7 d after reperfusion (i.e., the SMC-absent region was again populated with DsRed⁺ SMCs; Fig. 5f).

The phenomenon of SMC loss also occurred when a 2-h MCAO was applied to juvenile mice (P19–P24) via the intraluminal suture method (ischemic region, SMC survival = $67.5 \pm 2.5\%$; control region in contralateral hemisphere, survival = $96.6 \pm 1.0\%$, $n = 7$ mice; Supplementary Fig. 12). In adult mice, the SMC remained almost intact in the ischemic region (survival = $97.8 \pm 0.6\%$, $n = 4$ mice). To further investigate the mechanism of SMC loss in the ischemic brain, we stained the whole brain with anti- α SMA and observed a decrease in α SMA signal in DsRed-absent regions in some arteries or arterioles (Supplementary Fig. 13). DsRed loss was likely due to the death and/or severe damage of SMCs because we often observed membrane blebbing and intracellular vacuoles in SMCs during occlusion (Fig. 5f, Supplementary Fig. 14, and Supplementary Video 4).

DISCUSSION

Compared with conventional approaches, SIMPLE has broad applicability in studies of the neuron–glia–vasculature network

under ischemia. First, SIMPLE can reversibly occlude microvessels, for example, arterioles or venules. Second, SIMPLE can induce focal ischemic stroke in awake or freely moving animals without anesthesia or surgery of the skull or large arteries. This can be challenging to achieve by conventional strategies in which animals are required to remain under anesthesia or undergo a thinned-skull or open-skull procedure, which may contribute to secondary injury. Third, SIMPLE can control the duration of microvessel occlusion for live-imaging studies from occlusion onset through reperfusion. Hence, SIMPLE provides researchers an avenue to mimic transient ischemic attack, which can occur in the ‘healthy’ human brain but is difficult to model in mice³³.

Perinatal arterial ischemic stroke is common in infants (incidence, 1/5,000) and has been a frequent cause of long-term neurological disability in children³⁴. However, research progress on perinatal or neonatal stroke has been hindered owing to the lack of efficient strategies to precisely produce focal ischemic stroke for mechanistic studies²². SIMPLE can be applied to induce reversible focal ischemia in mice at any postnatal age, especially perinatal (P0–P3) and neonatal (P4–P9) mice, which is an advantage of this technique over conventional approaches.

In addition, SIMPLE provides a way to induce microinfarcts. Postmortem results from the brains of patients with dementia have shown many microinfarcts³⁵ with diameters of 0.1 to 1 mm^{15,36}. Infarcts produced by SIMPLE are usually smaller than 1.5 mm, which facilitates a microinfarct strategy to study brain injury and repair coupled with live-imaging technology. In preliminary experiments, we used SIMPLE to produce a microinfarct in the motor cortex and assessed mouse motor behavior using the cylinder test and forelimb flexion test. We did not observe obvious behavior defects in juvenile or adult mice (data not shown). Given that behavior readouts are among the most important evaluations for brain repair and recovery, this is a weakness of SIMPLE. Because of magnet placement on the mouse skull, the microinfarcts produced by SIMPLE are located at surface cortical regions (layers 1–4); hence, SIMPLE cannot be used to produce infarcts in deep brain regions.

Finally, to our knowledge this is the first report to demonstrate substantial differences in SMC pathology between the adult and juvenile brain after ischemia. SMCs are one of the three major cell types of the brain vasculature, and SMC loss in arteries or arterioles after ischemia might disrupt the neurovascular unit, which could lead to arterial reactivity to sensory stimulation or blood pressure change. Because SMCs are linked via gap junctions³⁷, we speculate that the relatively greater SMC loss in young animals might cause defects in constriction tone of arteries or arterioles that lead to reduced blood flow. The phenomenon that SMCs in the developing brain have such disparate fates under ischemia—and the question of how this may contribute to long-term cerebrovascular regulation and cognitive development—merit further investigation.

METHODS

Methods, including statements of data availability and any associated accession codes and references, are available in the [online version of the paper](#).

Note: Any Supplementary Information and Source Data files are available in the online version of the paper.

ACKNOWLEDGMENTS

We thank W.Z. Sun, L.J. Wu, H. Lü, and L.J. He for advice on live imaging; J. Zheng and A. Fu for advice on MPs; M. Dellinger for advice on H.E. staining; D. Xu and H. Cai for advice on MRI; B. Zhou, I. Shimada, M. Acar, and M. Chen for input concerning SMCs, MCAO and FJC staining; W.L. Du's input for MCAO surgery; T. Taylor, H. Zhu, J.D. Chen, Z.H. Zhang, Z.P. Hu, G.E. Cai, M. Goldberg, F. Chen, L. Smith, and J. Long as well as colleagues at CRI for critical discussion and reading of the manuscript. This work is supported by the National Basic Research Program of China (No. 2015CB352006) and the Science Fund for Creative Research Group of China (No. 61121004) to W.Z.; CRI start-up funds and NINDS K99/R00 (RO0NS073735) to W.-P.G.; NIH Director's New Innovator Award (DP2-NS082125) to B. Cui, American Heart Association (14SDG18410020) and NINDS (NS088555) to A.M.S.; and the Dr. Jack Krohmer Professorship in Radiation Physics for X.S. W.-P.G. is a recipient of an NINDS Pathway to Independence Award. W.L. is a recipient of an American Heart Association Postdoctoral Fellowship Award.

AUTHOR CONTRIBUTIONS

W.-P.G., B. Cui, and J.-M.J. conceived the project, and J.-M.J. performed most of the animal experiments and analyzed data. P.D.C. characterized properties of magnets. W.-P.G., X.G., B. Ci, E.J.P., W.L., A.M., G.H., A.K., and W.Z. performed the other experiments. W.-P.G., J.-M.J., P.D.C., X.G., B. Cui, X.S., A.M.S., and S.-H.Y. designed the experiments. W.-P.G., J.-M.J., X.G., P.D.C., B. Cui, A.M., and G.H. wrote the manuscript. All authors reviewed and edited the manuscript.

COMPETING FINANCIAL INTERESTS

The authors declare no competing financial interests.

Reprints and permissions information is available online at <http://www.nature.com/reprints/index.html>.

- Mozaffarian, D. *et al.* Heart disease and stroke statistics—2015 update: a report from the American Heart Association. *Circulation* **131**, e29–e322 (2015).
- Durukan, A. & Tatlisumak, T. Acute ischemic stroke: overview of major experimental rodent models, pathophysiology, and therapy of focal cerebral ischemia. *Pharmacol. Biochem. Behav.* **87**, 179–197 (2007).
- Koizumi, J., Yoshida, Y., Nakazawa, T. & Ooneda, G. Experimental studies of ischemic brain edema. 1. A new experimental model of cerebral embolism in rats in which recirculation can be introduced in the ischemic area. *Jpn. J. Stroke* **8**, 1–8 (1986).
- Longa, E.Z., Weinstein, P.R., Carlson, S. & Cummins, R. Reversible middle cerebral artery occlusion without craniectomy in rats. *Stroke* **20**, 84–91 (1989).
- Luo, W., Wang, Z., Li, P., Zeng, S. & Luo, Q. A modified mini-stroke model with region-directed reperfusion in rat cortex. *J. Cereb. Blood Flow Metab.* **28**, 973–983 (2008).
- Overgaard, K. *et al.* A rat model of reproducible cerebral infarction using thrombotic blood clot emboli. *J. Cereb. Blood Flow Metab.* **12**, 484–490 (1992).
- Niessen, F., Hilger, T., Hoehn, M. & Hossmann, K.A. Differences in clot preparation determine outcome of recombinant tissue plasminogen activator treatment in experimental thromboembolic stroke. *Stroke* **34**, 2019–2024 (2003).
- Watson, B.D., Dietrich, W.D., Busto, R., Wachtel, M.S. & Ginsberg, M.D. Induction of reproducible brain infarction by photochemically initiated thrombosis. *Ann. Neurol.* **17**, 497–504 (1985).
- Watson, B.D., Prado, R., Veloso, A., Brunschwig, J.P. & Dietrich, W.D. Cerebral blood flow restoration and reperfusion injury after ultraviolet laser-facilitated middle cerebral artery recanalization in rat thrombotic stroke. *Stroke* **33**, 428–434 (2002).
- Seto, A. *et al.* Induction of ischemic stroke in awake freely moving mice reveals that isoflurane anesthesia can mask the benefits of a neuroprotection therapy. *Front. Neuroenergetics* **6**, 1 (2014).
- Robinson, M.J., Macrae, I.M., Todd, M., Reid, J.L. & McCulloch, J. Reduction of local cerebral blood flow to pathological levels by endothelin-1 applied to the middle cerebral artery in the rat. *Neurosci. Lett.* **118**, 269–272 (1990).
- Dirnagl, U. Bench to bedside: the quest for quality in experimental stroke research. *J. Cereb. Blood Flow Metab.* **26**, 1465–1478 (2006).
- Nishimura, N. *et al.* Targeted insult to subsurface cortical blood vessels using ultrashort laser pulses: three models of stroke. *Nat. Methods* **3**, 99–108 (2006).
- Sigler, A., Goroshkov, A. & Murphy, T.H. Hardware and methodology for targeting single brain arterioles for photothrombotic stroke on an upright microscope. *J. Neurosci. Methods* **170**, 35–44 (2008).
- Shih, A.Y. *et al.* The smallest stroke: occlusion of one penetrating vessel leads to infarction and a cognitive deficit. *Nat. Neurosci.* **16**, 55–63 (2013).
- Fluri, F., Schuhmann, M.K. & Kleinschnitz, C. Animal models of ischemic stroke and their application in clinical research. *Drug Des. Devel. Ther.* **9**, 3445–3454 (2015).
- Karimi, Z., Karimi, L. & Shokrollahi, H. Nano-magnetic particles used in biomedicine: core and coating materials. *Mater. Sci. Eng. C Mater. Biol. Appl.* **33**, 2465–2475 (2013).
- Davis, M.E., Chen, Z.G. & Shin, D.M. Nanoparticle therapeutics: an emerging treatment modality for cancer. *Nat. Rev. Drug Discov.* **7**, 771–782 (2008).
- Jung, S. *et al.* Analysis of fractalkine receptor CX(3)CR1 function by targeted deletion and green fluorescent protein reporter gene insertion. *Mol. Cell. Biol.* **20**, 4106–4114 (2000).
- Herbst, J.F. & Croat, J.J. Neodymium-iron-boron permanent magnets. *J. Magn. Magn. Mater.* **100**, 57–78 (1991).
- Ferriero, D.M. Neonatal brain injury. *N. Engl. J. Med.* **351**, 1985–1995 (2004).
- Ashwal, S. & Pearce, W.J. Animal models of neonatal stroke. *Curr. Opin. Pediatr.* **13**, 506–516 (2001).
- Tsuji, M. *et al.* A novel reproducible model of neonatal stroke in mice: comparison with a hypoxia-ischemia model. *Exp. Neurol.* **247**, 218–225 (2013).
- Bederson, J.B. *et al.* Evaluation of 2,3,5-triphenyltetrazolium chloride as a stain for detection and quantification of experimental cerebral infarction in rats. *Stroke* **17**, 1304–1308 (1986).
- Schmued, L.C., Stowers, C.C., Scallet, A.C. & Xu, L. Fluoro-Jade C results in ultra high resolution and contrast labeling of degenerating neurons. *Brain Res.* **1035**, 24–31 (2005).
- Choudhury, G.R. & Ding, S. Reactive astrocytes and therapeutic potential in focal ischemic stroke. *Neurobiol. Dis.* **85**, 234–244 (2016).
- Iadecola, C. & Nedergaard, M. Glial regulation of the cerebral microvasculature. *Nat. Neurosci.* **10**, 1369–1376 (2007).
- Armulik, A., Genové, G. & Betsholtz, C. Pericytes: developmental, physiological, and pathological perspectives, problems, and promises. *Dev. Cell* **21**, 193–215 (2011).
- Carden, D.L. & Granger, D.N. Pathophysiology of ischaemia-reperfusion injury. *J. Pathol.* **190**, 255–266 (2000).
- Poittevin, M. *et al.* Smooth muscle cell phenotypic switching in stroke. *Transl. Stroke Res.* **5**, 377–384 (2014).
- Zhu, X., Bergles, D.E. & Nishiyama, A. NG2 cells generate both oligodendrocytes and gray matter astrocytes. *Development* **135**, 145–157 (2008).
- Hill, R.A. *et al.* Regional blood flow in the normal and ischemic brain is controlled by arteriolar smooth muscle cell contractility and not by capillary pericytes. *Neuron* **87**, 95–110 (2015).
- Albers, G.W. *et al.* Transient ischemic attack—proposal for a new definition. *N. Engl. J. Med.* **347**, 1713–1716 (2002).
- Nelson, K.B. Perinatal ischemic stroke. *Stroke* **38**, 742–745 (2007).
- Vinters, H.V. *et al.* Neuropathologic substrates of ischemic vascular dementia. *J. Neuropathol. Exp. Neurol.* **59**, 931–945 (2000).
- Sonnen, J.A. *et al.* Pathological correlates of dementia in a longitudinal, population-based sample of aging. *Ann. Neurol.* **62**, 406–413 (2007).
- Uehara, Y. & Burnstock, G. Demonstration of “gap junctions” between smooth muscle cells. *J. Cell Biol.* **44**, 215–217 (1970).

ONLINE METHODS

Animals. All animal experiments were carried out in accordance with protocols approved by the Institutional Animal Care and Use Committee at University of Texas Southwestern Medical Center. *NG2DsRedBAC*tg mice were originally from A. Nishiyama (University of Connecticut). Both male and female mice were included in this study.

Measurement of properties of micromagnets. Various cylindrical magnets made of neodymium-iron-boron (NdFeB; see **Supplementary Fig. 1**) were produced in China (Zhenli Co. Ltd, Jiaozuo, Henan). The magnets were 1–2 mm long and of differing diameter (0.3–3.0 mm). Magnets can be ordered directly from the company once the information regarding its materials (NdFeB), shape (cylindrical), size (length, 1–2 mm; diameter, 0.3–3.0 mm) is provided. Magnets were magnetized along the cylindrical axis. Magnetic field induction along the axis of the cylindrical magnets was measured using a Gauss meter (Model FM Bell 5080). The transverse field probe (STD58-0404) was placed flat on an optical bench; and the micromagnet, held within a capillary, was positioned at a calibrated distance from the surface of the probe using a 3D manipulator. Induction was measured as a function of distance from the magnet face (0.65–10 mm). These magnetic induction profiles were in good agreement with theoretically calculated profiles scaled by a factor of 1.5 (see details below). We then computed the magnetic field gradients from the scaled theoretical curves, which were noise free and provided the complete range (0–20 mm) of distances from the magnet surface.

The field along the axis of the cylindrical magnet at a distance d from the face of the magnet is calculated using the following formula³⁸, where L , R , and B_r are the length, radius, and residual flux density of the magnet, respectively.

$$B(d) = \frac{B_r}{2} \left(\frac{L+d}{\sqrt{(L+d)^2 + R^2}} - \frac{d}{\sqrt{d^2 + R^2}} \right)$$

The residual flux density B_r , which depends on the magnetic material, was not available for the custom-designed magnets in this study. However, commercial NdFeB magnets of different grades are known to have a varying range of B_r from 1.08–1.48 T, and we used an approximated value of 1.35 T in the calculations. The scaling of theoretical profiles to match the experimental measurement was primarily due to the approximated value of B_r in the calculations.

Measurement of properties of magnetic particles. MPs were made of ferrite oxide (magnetite) coated with polyethylene or dextran as we required. 180-nm MPs coated with PEG-2000 (Nanomag-D, PEG-2000, 180 nm, 10 mg/ml, MicroMod, Germany) were best suited for blood occlusion in mice. The nanoparticles can be directly ordered from the company once the information regarding their size and coated materials is provided. We measured the magnetization properties of MPs using alternating gradient magnetometry (Princeton Measurements Corp.). From the saturation magnetization and the magnetic moment provided by the manufacturer, we estimated the magnetic moment per particle (305 emu/nmol for 180-nm particles). Combining this with the magnetic gradient profiles, we computed the approximate force (moment \times gradient) that could be exerted by the cylindrical magnets on the 180-nm MPs. Although

the absolute force calculation was approximate owing to the approximated MP properties, the relative variation with respect to micromagnet geometry was accurate.

Magnetic resonance imaging of mice injected with magnetic particles. Coronal T2-weighted magnetic resonance images were collected on an Aspect Imaging M2TM 1.0 T System using the 43.5–45 MHz, 35 mm diameter radiofrequency (RF) mouse coil. Fast Spin Echo sequence was performed with the following parameters: repetition time = 6,000 ms; effective echo time = 103 ms; field of view = 80×100 mm², data matrix = 256×238 ; averaging = 2; slice = 1 mm. The field of view was centered on the liver. The images were collected preinjection and at 6, 30, 60, and 120 min postinjection of MPs. The MPs were intravenously injected into mice (5 μ g/g body weight). The mice were sedated (2% isoflurane) during the imaging acquisition. The imaging experiments were carried out with two mice.

Measurement of magnetic particle size. The MPs were suspended in water via 10-s mixing by a vortex mixer to ensure a uniform dispersion for the purpose of measuring MP hydrodynamic diameters with the Nanobrook Omni particle size analyzer (Brookhaven Instruments) using the dynamic laser scattering technique (90° angle of particle light scattering at wavelength 640 nm used by instrument). The effective diameter and polydispersity of each sample along with baseline indices were assessed using the manufacturer's software. Effective diameter is an average diameter calculated by the intensity of light scattered by each MP being analyzed in the sample. Polydispersity is a measure of nonuniformity in the MP sample, which is close to zero (0.000–0.020) for monodispersed or nearly monodispersed MPs, small (0.020–0.080) for narrowly distributed MPs, and large (>0.080) for broadly distributed MPs. We repeated these measurements three times.

In vitro measurement of the magnetic field and field gradient. The effect of the magnetic field and field gradient on the 180-nm MPs was monitored as follows. We made a 100 μ m-thick film of the MP solution in water sandwiched by two microscope coverslips (170 μ m) held by a spacer. The particles were imaged on an inverted microscope (60 \times objective) under dark-field conditions using oblique white-light illumination from the top. Using a 3D manipulator, we then positioned the cylindrical magnet at a specific distance from the surface of the top coverslip. Even when the 0.3-mm magnet was held far from the surface (\sim 1 mm), the field-induced magnetization in MPs was obvious from the formation of MP chains localized in a focal plane below the top coverslip. As the magnet approached the top coverslip, the magnetic force resulted in the rapid accumulation of MPs in the high-gradient region within seconds.

Toxicity test of magnetic particles in vitro. The 24-well plate was coated with BD Matrigel Matrix for 3.5 h in an incubator (37 °C with 5% CO₂). HEK293T cells were seeded at \sim 10% confluency and cultured overnight. On the second day, images were taken before cells were treated with MPs ($t = 0$ h; three groups: 1 mg/ml, 2 mg/ml, and control). Cells were then returned to the incubator and cultured for 4 h. After 4 h treatment, the medium with magnetic nanoparticles was removed, and the wells were washed with PBS twice before images were acquired ($t = 4$ h). The cells

were cultured for an additional 20 h in the incubator, and images were again acquired at 24 h ($t = 24$ h). HEK293T cell lines used in this study were obtained from J. Xu's lab (Children's Research Institute, UT Southwestern Medical Center) and were not further tested for mycoplasma contamination.

Measurement of basic physiological properties of mice. Adult mice were used for monitoring of vital signs before and after injection of MPs. Each mouse was rendered unconscious and kept under anesthesia using 1.5% isoflurane with carrier-air flow rate of 130 ml/min on a SomnoSuite small animal anesthesia system (Kent Scientific). Heart rate and SpO₂ were measured using the PhysioSuite physiological monitoring system (Kent Scientific) with a mouse paw pulse oximeter sensor. Body temperature was measured using a rectal probe connected to PhysioSuite. Each mouse was maintained under anesthesia for ~5 min to obtain a stable reading of heart rate and SpO₂. Then, respiration rate was manually counted. Each mouse was transferred back to its home cage after monitoring of vital signs. All mice were monitored before injection and 3 h, 24 h, and 4 d postinjection of MPs ($n = 7$ mice) or PBS ($n = 7$).

Blood glucose measurement. A restrainer was used to restrain conscious mice. Glucose level in one droplet of blood collected from the tails was measured with a glucometer (Bayer, Contour). Glucose level was measured before injection (control, day 1) and after injection of MPs (days 2, 3, 5, and 22).

Blood CO₂ measurement. Blood (~75 μ l) was collected from the retro-orbital sinus with a heparin-coated capillary tube (Fisher Scientific). Supernatant blood plasma was separated after blood was centrifuged (1,500 \times g, 20 min, 4 °C). The level of blood carbon dioxide (e.g., carbonate, ECO₂) in blood plasma was measured with a VITROS-250 Chemistry Analyzer (Ortho-Clinical Diagnostics) at the Mouse Metabolic Phenotyping Core at UT Southwestern Medical Center. ECO₂ was measured before and after injection of MPs (day 1 as control and days 5, and 22).

Injection of magnetic particles into the hippocampus *in vivo*. MPs (10 μ g) suspended in 1 μ l PBS were injected into the hippocampus of *CX₃CR1-GFP* knock-in mice and transgenic *Thy1-tdTomato* mice (produced in our laboratory) under anesthesia. As a control, 1 μ l PBS was injected into the hippocampus of the contralateral hemisphere. At 5 to 7 d after injection, each brain was fixed (4% PFA) for further analysis. We analyzed spine density of apical dendrites in hippocampal CA1 neurons of *Thy1-tdTomato* mice and microglial density in *CX₃CR1-GFP* mice.

Fluorescent labeling of blood cells. Labeling was conducted as previously reported³⁹ with some modifications. Briefly, one to two drops (~20–30 μ l) of blood were collected from the retro-orbital sinus of each mouse⁴⁰ with a microcentrifuge tube containing 500 μ l Hank's Balanced Salt Solution (HBSS) with 10 mM EDTA. The whole blood was centrifuged at 300 \times g for 5 min. After the supernatant was removed, the pellet was resuspended in 1 ml HBSS containing 7 μ M DiO (ThermoFisher Scientific). Cells were then incubated at 37 °C for 15 min. Labeled blood cells were washed twice with HBSS and then centrifuged as above and resuspended in 300 μ l HBSS. Approximately 50 μ l solution with

DiO-labeled cells was injected back into the same mouse via the tail vein. This procedure was done 1–2 d before or shortly before the induction of ischemic stroke with MPs.

Time-lapse imaging *in vivo*. DsRed-expressing SMCs in the brain of *NG2DsRedBAC* transgenic mice were imaged on an upright Zeiss LSM710 NLO two-photon excitation microscope equipped with an objective 20 \times /1.0 (differential interference contrast, VIS-IR). Cells were scanned with XYZ mode for time-lapse imaging as we previously reported⁴¹. Frame interval was 1–5 min for 30–100 frames. For line scanning, frequency was 1 ms/frame. During imaging, the body temperature of each mouse was maintained with a homemade heating pad (10 \times 5 cm). DsRed was excited with a laser at 543 nm or a 930–960 nm IR-laser. Additional images were taken every 6–12 h in the following week. During imaging, mice were anaesthetized with 1–2% isoflurane.

Occlusion with micromagnets without thinned-skull preparation. Mice (<P28) were anesthetized with isoflurane, and a 5-mm incision in the skin was made along the midline of the head. A cylindrical micromagnet was immobilized on top of the skull with superglue after incision. MPs, 80–150 μ g/g body weight in 150 μ l PBS, were administered via tail-vein injection when mice were fully conscious (without anesthesia and restrained by a mouse restrainer). Before injection, a solution with MPs was mixed thoroughly. For experiments in **Figure 2e**, at 3–60 min postinjection, mice (P16–P23) were sacrificed with overdose of isoflurane. To avoid bleeding that might partially perturb MP aggregation, we removed the skull from these sacrificed mice without decapitation, and images were acquired (**Fig. 2b,d,e**). For occlusion in perinatal and neonatal mice, MPs were injected at the superficial temporal vein as reported⁴² (dose = 80–150 μ g/g body weight). Hypothermia was used to control anesthetic depth when surgery was performed on perinatal and neonatal pups (**Fig. 3a**).

Occlusion with micromagnets after thinned-skull preparation. Occlusions in **Figures 1d–f** and **5** were produced in mice that had undergone a thinned-skull preparation. On day 1, mice were anesthetized with a mixture of ketamine (80–100 mg/kg) and xylazine (10–12 mg/kg). After removing scalp fur, we removed a 1 cm² patch of scalp to expose mouse skull. After attaching the metal plate with dental cement, we thinned a 2-mm square area on the skull with a microdrill until the thickness was ~20–50 μ m⁴³. DiO-labeled blood cells (in whole blood, see above) were injected into the tail vein. Mice were restrained on an imaging setup on day 2 for live imaging. Micromagnets (0.3 or 0.5 mm) were held via a glass filament and moved toward the targeted microvessels through a motorized micromanipulator (MP285). Under a microscope, an occlusion (with dark MPs) was immediately observed after tail-vein injection of MPs. Images were acquired either with a Nikon SMZ-18 stereoscope or Zeiss NLO710 confocal microscope before occlusion, during occlusion, and after removal of micromagnets. During imaging, mice were maintained under anesthesia by sustained perfusion of isoflurane (1–2%).

In experiments in **Figure 5**, we used a very small magnet (diameter, 0.3–0.5 mm). The magnet was held with a glass electrode (the same electrode generally used for whole-cell patch clamping). The electrode tip was cut so that the magnet could be attached. The angle between the magnet and mouse skull was

~30–45°. The manipulation with the small magnet shown in the figure did not produce a typical stroke core. Only 2–3 arterioles (diameter > 50 µm) could be blocked in any single experiment.

Brain vasculature imaging with latex blue. Mice were anesthetized with a mixture of ketamine (80–100 mg/kg) and xylazine (10–12 mg/kg). After exposing the heart, we slowly injected 5–10 ml blue latex dye (Connecticut Valley Biological Supply) into the left ventricle with a 25-ml syringe after cutting the right atrium. The brain was then removed and fixed with 4% paraformaldehyde overnight before imaging.

Measurement of blood flow with laser Doppler flowmetry. C57BL/6 mice were anesthetized with ketamine–xylazine on day 1, and a 10-mm incision was made along the midline of the head. Using superglue, a magnet was attached to the intact skull of juvenile mice or thinned skull of adult mice at the location above the distal MCA. The scalp was sutured before each mouse was returned to its home cage. Mice were anesthetized with 1–2% isoflurane on day 2. Baseline blood flow at selected locations around the magnet was measured with a probe (moorVMS-LDF laser Doppler monitor and VP4 needle probe, Moor Instruments, UK). After completing the first measurement, mice were left alone in a cage until they were fully conscious. After 15–30 min, MPs were injected via tail vein; and 30–60 min thereafter, blood flow was again measured at the same locations. Reperfusion rate was measured at immediately (~2 min) and 40 min after the magnet was removed from the skull with forceps.

Hematoxylin and eosin staining. Cryosections of fixed mouse brains (50 µm) were stained with 0.1% Mayer's hematoxylin for 20 s. After rinsing with running water for 5 min, each section was dipped in 0.5% eosin (diluted in 95% ethanol) and then rinsed with water as above. After dehydration with 50%, 70%, 95%, and 100% ethanol, the sections were cleared with pure xylene. Images were taken with an inverted microscope.

TTC staining. Mice ($n = 6$) that had undergone a 1-h occlusion of blood vessels were sacrificed at different time points (Fig. 4). The infarct area was determined by TTC staining at 1 h, 5 h, and 48 h after occlusion. Briefly, mice were sacrificed with overdose of isoflurane. After decapitation, each brain was dissected rapidly and sliced with a blade in PBS. Transverse slices (1 mm in thickness) were then maintained in a chamber. Brain slices were incubated in warm 2% TTC (in PBS) in a 37 °C water bath for 15 min. Brain slices were fixed with 4% paraformaldehyde overnight. After washing with PBS, images were taken with a Nikon SMZ-18 stereomicroscope.

Fluoro-Jade C staining. Mice ($n = 6$) that had been subjected to a 40-min occlusion of blood vessels were perfused transcardially with 4% paraformaldehyde at 72 h after occlusion. Degenerating neurons were detected with Fluoro-Jade C staining as described²⁵. Briefly, each brain was sliced into 20-µm sections and then immersed in 100% ethanol for 3 min, 70% ethanol for 1 min, distilled water for 1 min, and 0.06% potassium permanganate (KMnO₄) for 10 min and then incubated in a solution containing 0.0001% Fluoro-Jade C and 0.1% acetic acid for 10 min at room temperature. The sections were mounted with DPX (Sigma), a nonaqueous, styrene-based mounting medium.

Immunostaining. Fixed mouse brains were sectioned with a cryostat (model CM3050S, Leica) or Vibratome (50–70 µm, Leica, VT 1000S). Sections were stained as we described previously⁴¹. Briefly, sections were permeabilized with 0.25% Triton X-100 in PBS and then blocked with 5% bovine serum albumin and 3% normal goat serum with 0.125% Triton X-100 in PBS for 2 h. Primary antibodies against GFAP (1:300, rabbit, Sigma) and αSMA (1:200, rabbit, polyclonal, Abcam) were incubated with brain sections for 24–48 h at 4 °C. In conjunction with staining with Hoechst 33342 or DAPI (0.5 µg/ml, Thermo Fisher Scientific), brain sections were incubated with secondary antibodies conjugated with Alexa488 (1:750 dilution, Thermo Fisher Scientific) for 2 h at room temperature (22–25 °C). Sections were mounted with the antifade mounting medium Fluoro-Gel (EMS), and images were acquired with a Zeiss LSM710NLO confocal microscope. At least five brain sections were used for each independent immunostaining experiment. For staining in **Supplementary Figure 12**, whole brains were permeabilized with 1% Triton-X (overnight at 4 °C) followed by a 3-d incubation with anti-αSMA. After washing three times with PBS, each brain was incubated with Hoechst 33342 (0.5 µg/ml) and secondary antibody conjugated with Alexa488 (1:100 dilution) for 3 h at room temperature.

MCAO. Mice were anesthetized with a mixture of ketamine (80–100 mg/kg) and xylazine (10–12 mg/kg), and body temperature was maintained during surgery with a heating pad. A midline neck incision was made, the left common carotid artery was carefully separated from the vagus nerve, and the artery was ligated using a 5.0-string. A second knot was made on the left external carotid artery. The left internal carotid artery (ICA) was isolated, and a knot was left loose with a 5.0-string. This knot was not tightened until the intraluminal insertion was done. A small hole was cut on the common carotid artery before it was bifurcated to the external carotid artery and ICA. A silicon-coated monofilament (tip diameter = 150 µm for juveniles, 230 µm for adults, Doccol Corporation) was inserted into the ICA until it stopped at the origin of the MCA in the circle of Willis. The third knot on the ICA was closed to fix the filament in position. During MCA occlusion (2 h), mice were kept in a warm cage in which the temperature was maintained at 35 °C.

Data availability. The data sets generated during and/or analyzed during the current study are available from the corresponding author on reasonable request.

38. Camacho, J.M. & Sosa, V. Alternative method to calculate the magnetic field of permanent magnets with azimuthal symmetry. *Rev. Mex. Fis. E* **59**, 8–17 (2013).
39. van de Ven, A.L., Kim, P., Ferrari, M. & Yun, S.H. Real-time intravital microscopy of individual nanoparticle dynamics in liver and tumors of live mice. *Protoc. Exch.* <http://dx.doi.org/10.1038/protex.2013.049> (2013).
40. Golde, W.T., Gollobin, P. & Rodriguez, L.L. A rapid, simple, and humane method for submandibular bleeding of mice using a lancet. *Lab Anim. (NY)* **34**, 39–43 (2005).
41. Ge, W.P., Miyawaki, A., Gage, F.H., Jan, Y.N. & Jan, L.Y. Local generation of glia is a major astrocyte source in postnatal cortex. *Nature* **484**, 376–380 (2012).
42. Sands, M.S. & Barker, J.E. Percutaneous intravenous injection in neonatal mice. *Lab. Anim. Sci.* **49**, 328–330 (1999).
43. Xu, H.T., Pan, F., Yang, G. & Gan, W.B. Choice of cranial window type for *in vivo* imaging affects dendritic spine turnover in the cortex. *Nat. Neurosci.* **10**, 549–551 (2007).